



HAL
open science

Title External α carbonic anhydrase and solute carrier 4 (SLC4)

Wenmin Huang, Shijuan Han, Hongsheng Jiang, Shuping Gu, Wei Li, Brigitte Gontero, S.C. Maberlly

► **To cite this version:**

Wenmin Huang, Shijuan Han, Hongsheng Jiang, Shuping Gu, Wei Li, et al.. Title External α carbonic anhydrase and solute carrier 4 (SLC4). *Journal of Experimental Botany*, 2020, 71 (19), pp.6004-6014. 10.1093/jxb/eraa351 . hal-02969009

HAL Id: hal-02969009

<https://amu.hal.science/hal-02969009>

Submitted on 16 Oct 2020

HAL is a multi-disciplinary open access archive for the deposit and dissemination of scientific research documents, whether they are published or not. The documents may come from teaching and research institutions in France or abroad, or from public or private research centers.

L'archive ouverte pluridisciplinaire **HAL**, est destinée au dépôt et à la diffusion de documents scientifiques de niveau recherche, publiés ou non, émanant des établissements d'enseignement et de recherche français ou étrangers, des laboratoires publics ou privés.

1 **Title** External α carbonic anhydrase and solute carrier 4 (SLC4)
2 bicarbonate transporter are required for HCO_3^- uptake in a freshwater
3 angiosperm

4

5 **Authors**

6 Wenmin Huang^{1,2}, Shijuan Han^{1,3}, Hongsheng Jiang¹, Shuping Gu⁴, Wei Li^{1,*}, Brigitte
7 Gontero^{2,*}, Stephen C. Maberly^{5,*}

8 ¹Key Laboratory of Aquatic Botany and Watershed Ecology, Wuhan Botanical Garden,
9 Center of Plant Ecology, Core Botanical Gardens, Chinese Academy of Sciences,
10 Wuhan 430074, China

11 ²Aix Marseille Univ CNRS, BIP UMR 7281, IMM, FR 3479, 31 Chemin Joseph
12 Aiguier, 13402 Marseille Cedex 20, France

13 ³University of Chinese Academy of Sciences, Beijing 100049, China

14 ⁴Shanghai Sequen Bio-info Studio, Shanghai, 200092, China

15 ⁵Lake Ecosystems Group, UK Centre for Ecology & Hydrology, Lancaster
16 Environment Centre, Library Avenue, Bailrigg, Lancaster LA1 4AP, UK

17 *Correspondence: Wei Li (liweili@wbgcas.cn), Brigitte Gontero
18 (bmeunier@imm.cnrs.fr), Stephen C. Maberly (scm@ceh.ac.uk)

19

20 **Highlight**

21 Acquisition of HCO_3^- in *Ottelia alismoides*, relies on co-diffusion of CO_2 and HCO_3^-
22 through the boundary-layer, conversion of HCO_3^- to CO_2 at the plasmalemma by $\alpha\text{CA-}$
23 1 and transport by SLC4.

24

25

26 **Abstract**

27 The freshwater monocot *Ottelia alismoides* is the only known species to operate three
28 CO₂ concentrating mechanisms (CCMs): constitutive HCO₃⁻-use and C4
29 photosynthesis, and facultative Crassulacean acid metabolism, but the mechanism of
30 HCO₃⁻ use is unknown. We found that the inhibitor of an anion exchange (AE) protein,
31 4,4'-diisothio-cyanatostilbene-2,2'-disulfonate (DIDS), prevented HCO₃⁻ use but also
32 had a small effect on CO₂ uptake. An inhibitor of external carbonic anhydrase (CA),
33 acetazolamide (AZ), reduced the affinity for CO₂ uptake but also prevented HCO₃⁻ use
34 via an effect on the AE protein. Analysis of mRNA transcripts identified a homologue
35 of solute carrier 4 (SLC4) responsible for HCO₃⁻ transport, likely to be the target of
36 DIDS, and a periplasmic α CA-1. We produced a model to quantify the contribution of
37 the three different pathways involved in inorganic carbon uptake. Passive CO₂ diffusion
38 dominates inorganic carbon uptake at high CO₂ concentrations. However, as CO₂
39 concentrations fall, two other pathways become predominant: conversion of HCO₃⁻ to
40 CO₂ at the plasmalemma by α CA-1 and, transport of HCO₃⁻ across the plasmalemma
41 by SLC4. These mechanisms allow access to a much larger proportion of the inorganic
42 carbon pool and continued photosynthesis during periods of strong carbon depletion in
43 productive ecosystems.

44

45 **Keywords**

46 anion exchanger, bicarbonate, carbonic anhydrase (CA), CO₂ concentrating
47 mechanisms (CCMs), inorganic carbon acquisition, *Ottelia alismoides*, pH drift,
48 photosynthesis, solute carrier 4 (SLC4)

49 **Introduction**

50 Macrophytes form the base of the freshwater food web and are major contributors to
51 primary production, especially in shallow systems (Silva *et al.*, 2013; Maberly and
52 Gontero, 2018). However, the supply of CO₂ for photosynthesis in water is potentially
53 limited by the approximately 10,000 lower rate of diffusion compared to that in air
54 (Raven, 1970). This imposes a large external transport resistance through the boundary
55 layer (Black *et al.*, 1981), that results in the K_{1/2} for CO₂ uptake by macrophytes to be
56 100-200 μM, roughly 6-11 times air-equilibrium concentrations (Maberly and Madsen,
57 1998). Furthermore, in productive systems the concentration of CO₂ can be depleted
58 close to zero (Maberly and Gontero, 2017). Freshwater plants have evolved diverse
59 strategies to minimize inorganic carbon (C_i) limitation (Klavnsen *et al.*, 2011) including
60 the active concentration of CO₂ at the active site of ribulose-1,5-bisphosphate
61 carboxylase/oxygenase (Rubisco), collectively known as CO₂ concentrating
62 mechanisms (CCMs). The most frequent CCM in freshwater plants is based on the
63 biophysical uptake of bicarbonate (HCO₃⁻), which is present in ~50% of the species
64 tested (Maberly and Gontero, 2017; Iversen *et al.*, 2019). While CO₂ can diffuse
65 through the cell membrane passively, HCO₃⁻ use requires active transport because the
66 plasmalemma is impermeable to HCO₃⁻ and the negative internal membrane potential
67 (Denny and Weeks, 1970) produces a large electrochemical gradient resisting passive
68 HCO₃⁻ entry (Maberly and Gontero, 2018).

69 Detailed studies of the mechanisms of HCO₃⁻ use have been carried out in
70 microalgae, marine macroalgae, seagrasses and to a lesser extent, freshwater
71 macrophytes (Giordano *et al.*, 2005). Direct uptake/transport of HCO₃⁻ can occur via
72 an anion exchanger (AE) located at the plasmalemma (Sharkia *et al.*, 1994). Inhibition
73 of this protein by the membrane impermeable and highly specific chemical, 4,4'-
74 diisothiocyanatostilbene-2,2'-disulfonate (DIDS), has confirmed its effect in a range of
75 marine macroalgae and seagrasses (Drechsler *et al.*, 1993; Björk *et al.*, 1997; Fernández
76 *et al.*, 2014). Genomic studies have found probable AE proteins, from the solute carrier
77 4 (SLC4) family bicarbonate transporters (Romero *et al.*, 2013), in marine microalgae
78 (Nakajima *et al.*, 2013; Poliner *et al.*, 2015).

79 Carbonic anhydrase (CA) is a ubiquitous enzyme and is present in photosynthetic
80 organisms. It interconverts CO₂ and HCO₃⁻, maintaining equilibrium concentrations
81 when rates of carbon transformation are high (Moroney *et al.*, 2001; Dimario *et al.*,

82 2018). External carbonic anhydrase (CA_{ext}) is inhibited by the impermeable inhibitor
83 acetazolamide (AZ). The widespread nature of CA_{ext} is demonstrated by the inhibition
84 of rates of photosynthesis in a range of aquatic photoautotrophs (James and Larkum,
85 1996; Larsson and Axelsson, 1999; Moroney *et al.*, 2011; Tachibana *et al.*, 2011; van
86 Hille *et al.*, 2014; Fernández *et al.*, 2018). In many marine species, both CA_{ext} and an
87 AE protein are implicated in the uptake of HCO₃⁻ but very little is known about
88 freshwater macrophytes (Millhouse and Strother, 1986; Beer and Rehnberg, 1997;
89 Björk *et al.*, 1997; Gravot *et al.*, 2010; Tsuji *et al.*, 2017).

90 *Ottelia alismoides* (L.) Pers., a member of the monocot family Hydrocharitaceae,
91 possesses two biochemical CCMs: constitutive C4 photosynthesis and facultative
92 Crassulacean Acid Metabolism (CAM; Zhang *et al.*, 2014; Shao *et al.*, 2017; Huang *et*
93 *al.*, 2018). The leaves of *O. alismoides* comprise epidermal and mesophyll cells that
94 contain chloroplasts and large air spaces but lack Kranz anatomy (Han *et al.*, 2020).
95 Although it is known that it can use HCO₃⁻ in addition to CO₂, little is known about the
96 mechanisms responsible for HCO₃⁻ uptake. We have addressed this issue, with Ci
97 uptake measurements using the pH-drift technique, experiments with inhibitors of CA
98 and AE and analysis of transcriptomic data.

99 **Materials and methods**

100 *Plant material and growth conditions*

101 *O. alismoides* seeds were sown in soil from Donghu Lake, adjacent to the laboratory in
102 Wuhan, and covered with sterile tap water with an alkalinity of about 2.2 mequiv L⁻¹ as
103 described (Huang *et al.*, 2018). After a month, seedlings were placed in a 400-L tank
104 (64 cm deep) receiving natural daylight in a glasshouse on the flat roof of the laboratory.
105 The tap water in the tank was changed weekly and snails were removed daily. After
106 nearly two months, the plants in the tank had produced many mature leaves. pH and
107 temperature were measured every day with a combination pH electrode (E-201F,
108 Shanghai Electronics Science Instrument Co., China) connected to a Thermo Orion
109 Dual Star Benchtop pH/ISE Meter. The alkalinity was measured by Gran titration with
110 a standard solution of HCl. CO₂ concentrations were calculated from pH, alkalinity, and
111 temperature using the equations in Maberly (1996). Because of their high biomass the
112 plants generated high pH values (8.3-9.7) and low concentrations of CO₂ (0.11-6.15
113 μM) in the tank. Information of the conditions in the tank is shown in Supplementary

114 Table S1.

115 To examine whether HCO_3^- acquisition was affected by carbon limitation, in a
116 separate experiment *O. alismoides* was incubated at high and low CO_2 concentration
117 for 40 days in plastic containers within one of the tanks in the glasshouse as described
118 previously (Zhang *et al.*, 2014). The pH in the low CO_2 treatment (LC) ranged from 8.0
119 to over 9.8 and the CO_2 concentration ranged from 0.1 to 13 μM with a mean of 2.4 μM .
120 For the high CO_2 treatment (HC), CO_2 -saturated tap water was added to the buckets
121 twice each day in order to keep the pH between 6.7-6.8, producing CO_2 concentrations
122 between 481-1110 μM with a mean of 720 μM (Supplementary Table S1). These
123 different CO_2 acclimated leaves were used to detect the effect of AZ and DIDS on C_i
124 uptake rate and external CA activity.

125 *pH-drift experiments*

126 The pH-drift technique was used to determine the capacity of *O. alismoides* to utilize
127 HCO_3^- , and the effects of inhibitors (AZ and DIDS) on photosynthetic C_i uptake
128 (Maberly and Spence, 1983). Measurements were made in a glass and plastic chamber
129 (Maberly, 1990) containing 121 mL of 1 mM HCO_3^- comprising equimolar
130 concentration of NaHCO_3 and KHCO_3 , a pH electrode (model IP-600-9 Jenco
131 Instruments, USA) and an oxygen electrode (Unisense OX-13298). The chamber was
132 placed in a water bath maintained at $25 \pm 2 \text{ }^\circ\text{C}$ and illuminated from the side by fluorescent
133 tubes that provided $75 \mu\text{mol photon m}^{-2} \text{ s}^{-1}$ (400-700 nm, Li-Cor sensor connected to a
134 Li-Cor LI-1400 data logger). Prior to the start of the pH drift experiments, the leaves
135 were collected from the tank in the glasshouse in the morning to avoid possible
136 physiological differences caused by a light:dark rhythm of the plant, and then pieces of
137 ~ 1.1 g fresh weight (FW) of leaf tissue were cut and rinsed in the medium placed in a
138 constant temperature room at $25 \pm 2 \text{ }^\circ\text{C}$ for around 1-4 hours before use. The medium
139 in the incubation chamber was initially bubbled with N_2 to reduce O_2 concentration
140 $\sim 100 \pm 20 \mu\text{M}$, which was detected by the oxygen electrode connected to an Unisense
141 microsensor multimeter (Version 2.01) and recorded on a laptop computer. At the start
142 of all drift experiments, the pH of the medium was set to 7.6 with CO_2 -bubbled medium,
143 and the subsequent changes were measured with the pH electrode connected to a pH
144 meter (model 6311, Jenco Instruments, USA), and recorded on a monitor (TP-LINK,
145 TL-IPC42A-4). The pH-drifts, undertaken at least in triplicate, took 6-23 h to reach an
146 end point value (final pH), which was deemed to be achieved when the pH changed less

147 than 0.01 unit in one hour (Maberly, 1990). After each drift, the dry weight of the plant
148 material and the alkalinity of the medium were measured, allowing C_i concentrations
149 and C_i uptake rates to be calculated (Maberly and Spence, 1983). When photosynthetic
150 C_i uptake rates were plotted against the total carbon concentration (C_T) at which the
151 rate occurred, a two-phased response curve was observed. The linear response at higher
152 C_T concentration was the consequence of CO_2 use, and the extrapolated intercept with
153 the C_T axis corresponded to the CO_2 compensation point (Maberly and Spence, 1983).

154 *Effect of inhibitors on C_i -uptake and external CA activity*

155 Inhibitors were used in pH-drift experiments to determine their effect on C_i -uptake. A
156 stock solution of AZ (20 mM) was prepared by dissolving the solid in 20 mM NaOH
157 and 0.61 or 1.21 mL was injected into the chamber to produce final concentration of
158 0.1 or 0.2 mM respectively. Stock solutions of 30 mM DIDS, were prepared daily by
159 dissolving the powder in distilled water (Cabantchik and Greger, 1992), and 1.21 mL
160 was injected into the chamber to produce a final concentration of 0.3 mM. Both stock
161 solutions were kept in the dark at 4°C.

162 To check if the inhibitory effect of AZ on HCO_3^- uptake was reversible, we
163 performed three consecutive drifts using the same *O. alismoides* leaf cut longitudinally
164 into two halves. The first half was used as a control (first drift) without AZ. The second
165 half was treated with AZ (second drift). Subsequently, this leaf and chamber were
166 thoroughly rinsed with clean medium three times over ten minutes, and finally a post-
167 control (third drift), was performed without the inhibitor. All the pH-drifts were started
168 at pH 7.6 and stopped at pH 8.5 and replicated at least in triplicate.

169 *External CA activity*

170 The CA_{ext} activity was measured as in Fernández *et al.* (2018) with small modifications,
171 using commercial CA (Sigma, C4396) as a positive control and to check activity
172 linearity (Supplementary Fig. S1). A 50 mL plastic tube was placed inside a container
173 filled with ice that maintained the temperature at 0-4°C. Approximately 60 mg FW leaf
174 was placed in the tube containing 10 mL of buffer (pH 8.5): 50 mM Tris, 2 mM DTT,
175 15 mM ascorbic acid, 5 mM Na_2 -EDTA and 0.3% w/v polyvinylpyrrolidone (PVP).
176 Temperature and pH were simultaneously measured using a pH meter. The reaction was
177 started by rapidly introducing 5 mL of ice-cold CO_2 saturated water and pH was
178 recorded over time. The relative enzyme activity (REA) was determined using the

179 equation below:

$$180 \quad \text{REA} = (T_b/T_s) - 1 \quad (1)$$

181 where T_b and T_s are the times in seconds required for the pH to drop from pH 8.3
182 to 7.9 in the non-catalyzed (without sample) and catalyzed reactions, respectively. The
183 REA was expressed on a fresh weight basis. In the leaves grown at LC and HC, external
184 CA activity was measured in the presence of 0.1 mM and 0.2 mM AZ as well as 0.3
185 mM DIDS.

186 *Transcriptomic analysis*

187 CA_{ext} and AE proteins were searched for within a transcriptome dataset obtained from
188 *O. alismoides* acclimated to LC and HC (Huang *et al.*, 2018). Information of the
189 different CO_2 treatments is shown in Supplementary Table S1. Six samples (three HC
190 and three LC acclimated mature leaves) were used for second-generation sequencing
191 (SGS) for short but high-accuracy reads (Hackl *et al.*, 2014). Six other samples were
192 used for the third-generation sequencing (TGS) for longer sequences but lower-quality
193 reads (Roberts *et al.*, 2013).

194 Around 0.3 g fresh weight leaves were collected 30 minutes before the end of the
195 photoperiod, flash frozen in liquid N_2 and stored at $-80^\circ C$ before use. Total RNA was
196 extracted using a commercial kit RNAiso (Takara Biotechnology, Dalian, China). The
197 purified RNA was dissolved in RNase-free water, with genomic DNA contamination
198 removed using TURBO DNase I (Promega, Beijing, China). RNA quality was checked
199 with the Agilent 2100 Bioanalyzer (Agilent Technologies, Palo Alto, California). Only
200 the total RNA samples with RNA integrity numbers ≥ 8 were used to construct the
201 cDNA libraries in PacBio or Illumina HiSeq sequencing.

202 For TGS analysis, total RNA (2 μg) was reversely transcribed into cDNA using the
203 SMARTer PCR cDNA Synthesis Kit that has been optimized for preparing high-quality,
204 full-length cDNAs (Takara Biotechnology, Dalian, China), followed by size
205 fractionation using the BluePippin™ Size Selection System (Sage Science, Beverly,
206 MA). Each SMRT bell library was constructed using 1-2 μg size-selected cDNA with
207 the Pacific Biosciences DNA Template Prep Kit 2.0. SMRT sequencing was then
208 performed on the Pacific Bioscience sequel platform using the manufacturer's protocol.

209 For SGS analysis, cDNA libraries were constructed using a NEBNext® Ultra™
210 RNA Library Prep Kit for Illumina® (NEB, Beverly, MA, USA), following the
211 manufacturer's protocol. Qualified libraries were sequenced, and 150 bp paired-end

212 reads were generated (Illumina Hiseq 2500, San Diego, CA, USA).

213 The TGS subreads were filtered using the standard protocols in the SMRT analysis
214 software suite (<http://www.pacificbiosciences.com>) and reads of insert (ROIs) were
215 generated. Full-length non-chimeric reads (FLNC) and non-full-length cDNA reads
216 (NFL) were recognized through the identification of poly(A) signal and 5' and 3'
217 adaptors. The FLNC reads were clustered and polished by the Quiver program with the
218 assistance of NFL reads, producing high-quality isoforms (HQ) and low-quality
219 isoforms (LQ). The raw Illumina reads were filtered to remove ambiguous reads with
220 'N' bases, adaptor sequences and low-quality reads. Filtered Illumina data were then
221 used to polish the LQ reads using the proovread 213.841 software. The redundant
222 isoforms were then removed to generate a high-quality transcript dataset for *O.*
223 *alismoides*, using the program CD-HIT.

224 TransDecoder v2.0.1 (<https://transdecoder.github.io/>) was used to define the
225 putative coding sequence (CDS) of these transcripts. The predicted CDS were then
226 functional annotated and confirmed by BLAST, which was conducted against the
227 following databases: NR, NT, KOG, COG, KEGG, Swissprot and GO. For each
228 transcript in each database searched, the functional information of the best matched
229 sequence was assigned to the query transcript. The phylogenetic tree of α CA-1 isoforms
230 based on deduced CA peptide sequences from the NCBI, was analyzed with Geneious
231 software (Windows version 11.0, Biomatters Ltd, New Zealand). The location of the
232 protein was analyzed using Target P1 (Emanuelsson *et al.*, 2007;
233 <http://www.cbs.dtu.dk/services/TargetP/>).

234 *Statistical analysis*

235 All data presented in this study are the mean \pm SD. Mean final pH values were calculated
236 geometrically. One-way ANOVA was used to test for significant variation, after
237 homogeneity and normality were satisfied. Duncan's and Tukey's post-hoc tests were
238 used to test for significance among treatments while percentage data were compared
239 using a non-parametric Mann-Whitney test. The threshold of statistical significance
240 was set at $P < 0.05$. The data were analyzed using SPSS 16.0 (SPSS Inc., Chicago, IL,
241 USA).

242 **Results**

243 In control leaves, the pH drift end point was reached after nearly 24 hours at a mean pH

244 of 10.2 (Fig. 1, 2A) and a very low final CO₂ concentration of ~0.03 μM (about 450-
245 fold below air equilibrium, and at an oxygen concentration of about 353 μM, about 137%
246 of air-equilibrium; Fig. 2B) indicating that HCO₃⁻ had been used. In leaves treated with
247 AZ or DIDS, the pH drift stopped after 6 to 12 hours and the end point did not exceed
248 pH 9.3; final CO₂ concentrations were between 0.8 and 1.6 μM (Fig. 1, Fig. 2A, 2B),
249 indicating that HCO₃⁻ use had been inhibited. As a consequence of HCO₃⁻ use in control
250 leaves, rates of C_i uptake were about 40 μmol g⁻¹ DW h⁻¹ even at the very low CO₂
251 concentrations (Supplementary Fig. S2). The slope of C_i uptake vs concentration of
252 CO₂ between 15 and 40 μM in leaves treated with AZ was between 54.1% and 70.6%
253 lower than the control (P<0.05) and in leaves treated with DIDS, it was about 35%
254 lower than the control (P<0.05; Fig. 2C). In contrast, the intercept CO₂ compensation
255 points increased significantly as a result of the addition of AZ (Fig. 2D). The higher AZ
256 concentration treatments had a CO₂ compensation concentration close to 20 μM (at an
257 oxygen concentration of 163 μM) suggesting that CCM is absent. These results suggest
258 that AZ not only inhibited C_{Aext} but also inhibited the AE protein. The CO₂
259 compensation concentration in the presence of DIDS, at about 5 μM (at an oxygen
260 concentration of 232 μM, about 90% of air-equilibrium), was not significantly different
261 from the control but substantially lower than in the two AZ treatments (Fig. 2D). The
262 C_T/alkalinity quotient (the remaining total C_i at the end of the drift, C_T related to the
263 alkalinity) is a measure of the effectiveness of C_i depletion. A low quotient indicates
264 that a large proportion of the C_i pool is available for acquisition and vice versa. While
265 HCO₃⁻ use in control leaves allowed about half of the available inorganic carbon to be
266 accessible, in the AZ and DIDS treated leaves, a high quotient was obtained and only
267 between 11 and 16% of the available inorganic carbon was accessible (Fig. 2E).

268 Fig. 3 shows the C_i uptake rates at different CO₂ concentrations calculated from the
269 pH-drift experiments over a pH range from about 7.7 to 9.3. AZ inhibited C_i-uptake at
270 all the CO₂ concentrations (Fig. 3A), and both AZ concentrations inhibited C_i uptake
271 by between 70 and 76% when the concentrations of CO₂ were between 2.6 and 11 μM.
272 In contrast, DIDS did not affect C_i uptake at CO₂ concentrations above 4.2 μM but
273 inhibited C_i uptake by about 40% at CO₂ concentrations between about 1 and 4 μM

274 (Fig. 3B). The inhibitory effect caused by AZ at both concentrations, can be completely
275 reversed by washing since the post-control rates of C_i uptake were not significantly
276 different from the initial control ($P>0.05$; Fig. 4). This confirms that AZ does not
277 penetrate the plasmalemma (Moroney *et al.*, 1985) and thus that the observed effects
278 are linked to inhibition of CA_{ext} .

279 The inhibition of C_i uptake rates in the presence of 0.1 mM AZ and 0.3 mM DIDS
280 were not significantly different in leaves acclimated to HC *vs* LC, although there was a
281 slightly greater inhibition by 0.2 mM AZ in HC compared to LC leaves ($P<0.05$; Fig.
282 5A, 5B). CA_{ext} activity was present in both HC and LC leaves but it was greater in LC
283 leaves ($P<0.01$; Fig. 5C). CA_{ext} activity was inhibited by AZ: the 0.2 mM treatment
284 caused a greater inhibition than 0.1 mM AZ (Fig. 5D). DIDS had no effect on CA_{ext}
285 activity neither in HC nor in LC leaves. C_i uptake rates, measured at an initial CO_2
286 concentration of 12 μM , were broadly positively related to the activity of CA_{ext} ($R^2 =$
287 0.84 and 0.74 for HC and LC leaves respectively, $P<0.01$).

288 The inhibition of C_i uptake in *O. alismoides* by AZ and DIDS implied that both
289 CA_{ext} and anion exchange protein were present. This was characterized further using
290 transcriptomic analysis: mRNA for putative alpha carbonic anhydrase 1 ($\alpha CA-1$) and
291 HCO_3^- transporters were expressed. Fifty-three transcripts were functionally annotated
292 to CA according to sequence similarity and translated into 66 peptides. Six of these
293 peptides were homologous with $\alpha CA1$ based on a comparison of amino acid sequences
294 with the NCBI database and corresponded to four CA isoforms (Fig. 6A,
295 Supplementary Fig. S3). Isoform 1 in *O. alismoides* shows 60% and 61% identity with
296 the chloroplastic isoform X1 and X2 of $\alpha CA-1$ from the monocot *Musa acuminata*.
297 Isoforms 2, 3 and 4 show 58%, 55% and 56% identity with the isoform X1 from this
298 species, respectively, as well as 59%, 57% and 58% identity with the isoform X2.
299 However, according to Target P1 software, all the isoforms from *O. alismoides* were
300 predicted to be localized in the secretory pathway (Fig. 6B). The expression of the four
301 isoforms of putative $\alpha CA-1$, was not significantly different in HC and LC acclimated
302 leaves ($P>0.05$, Fig. 6C).

303 Unfortunately, transcripts of HCO_3^- transporters were not detected due to the lower
304 sensitivity of TGS, but were present in the dataset from SGS. Fifteen peptides
305 sequences (Supplementary Fig. S3) were inferred to be homologous to HCO_3^-
306 transporter family with the following dicot species in the database: *Artemisia annua*

307 (70.6-78.9%), *Corchorus olitorius* (73.1-85.7%), *Corchorus capsularis* (73.1-85.7%),
308 *Cynara cardunculus* (80.4-85.7%), *Lupinus albus* (73.22%), *Macleaya cordata* (76.2-
309 83.5%), *Parasponia andersonii* (74.0%), *Populus alba* (77.6%), *Prunus dulcis* (78.5-
310 82.4%), *Striga asiatica* (81.6-83.5%), *Theobroma cacao* (79.2-85.0%) and *Trema*
311 *orientale* (75.1-75.8%). This HCO₃⁻ transporter family contains Band 3 anion exchange
312 proteins, which also known as anion exchanger 1 or SLC4 member 1. Only partial
313 sequences could be deduced from our analysis and since the peptides for putative HCO₃⁻
314 transporters are membrane proteins, their location could not be predicted. The mRNA
315 expressions of all the transcripts for putative SLC4 HCO₃⁻ transporters were not
316 significantly different in HC and LC acclimated leaves (P>0.05, data not shown); the
317 expression-data for the highest expressed transcript for SLC4 HCO₃⁻ transporters is
318 presented in Fig. 6D.

319 Discussion

320 *O. alismoides* possesses three CCMs, including constitutive abilities to (i) use HCO₃⁻
321 and (ii) operate C4 photosynthesis, and a facultative ability to perform CAM when
322 acclimated to low CO₂ concentrations (Zhang *et al.*, 2014; Shao *et al.*, 2017; Huang *et al.*,
323 2018). We confirm here that this species has a constitutive ability to use HCO₃⁻, and
324 this allows it to exploit a large proportion of the Ci pool and drive CO₂ to very low
325 concentrations.

326 In this study, multiple lines of evidence show that an external CA, putative α CA-1,
327 plays a major role in Ci uptake in *O. alismoides*: (i) external CA activity was measured,
328 (ii) AZ inhibited Ci uptake with the slope of Ci uptake *vs* the concentration of CO₂
329 between 15 and 40 μ M being about a quarter of the control after treatment with 0.2 mM
330 AZ, (iii) transcripts of putative α CA-1 were detected. The CA was confirmed to be
331 external since (i) washing of leaves treated with AZ, restored CA activity and (ii) its
332 sequence bears a signal peptide consistent with a periplasmic location. External CA is
333 indeed widespread in photoautotrophs from marine and freshwater environments
334 (Moroney *et al.*, 2001; Dimario *et al.*, 2018). The green microalga *Chlamydomonas*
335 *reinhardtii* has three α CAs, of which two (Cah1 and Cah2) are localized in the
336 periplasmic space and one (Cah3) in the thylakoid membrane (Fujiwara *et al.*, 1990;
337 Karlsson *et al.*, 1998; Moroney and Chen, 1998). While CAs have the same catalytic
338 activity, their sequence identity could be very low among different classes (Jensen *et*

339 *al.*, 2019). The α CA-1 from *O. alismoides* has around 30% sequence identity with the
340 periplasmic Cah1 from *C. reinhardtii*. Many CAs are regulated by the concentration of
341 CO₂. The diatom *Phaeodactylum tricornutum* does not possess external CA, but the
342 internal CA (β -type CA) is CO₂ responsive and crucial for its CCM operation (Satoh *et al.*
343 *al.*, 2001; Harada *et al.*, 2005; Harada and Matsuda, 2005; Tsuji *et al.*, 2017). In the
344 marine diatom, *Thalassiosira pseudonana*, the two external CAs, δ -CA and ζ -CA, as
345 well as a recently identified chloroplastic ι -CA are induced by carbon limitation
346 (Samukawa *et al.*, 2014; Clement *et al.*, 2017; Jensen *et al.*, 2019). In contrast, the
347 putative α CA-1 in *O. alismoides* is constitutive and its expression was unaffected by
348 the CO₂ concentration. This is also true for Cah3 in the thylakoid lumen of *C.*
349 *reinhartii* (Karlsson *et al.*, 1998; Moroney and Chen, 1998), while the expression of
350 the periplasmic CA (Cah1) and the mitochondrial CAs (β -CA1 and β -CA2) are highly
351 CO₂-sensitive (Moroney and Chen, 1998).

352 We show that the anion exchange proteins, one group of the SLC4 family HCO₃⁻
353 transporters (Romero *et al.*, 2013), is involved in HCO₃⁻ uptake in *O. alismoides*. DIDS,
354 a commonly-used inhibitor of AE/SLC-type HCO₃⁻ transporters (Romero *et al.*, 2013)
355 significantly decreased the final pH of a drift, and increased the final CO₂ concentration
356 to about 0.8 μ M which is not substantially less than that expected in the absence of a
357 CCM: a terrestrial C₃ plant CO₂ compensation point of 36 μ L L⁻¹ (Bauer and Martha,
358 1981) is equivalent to about 1.2 μ M. Furthermore, transcripts of putative HCO₃⁻
359 transporter family in *O. alismoides* were found to contain Band 3 anion exchange
360 proteins (SLC4 member 1), and the peptides shared 70.6-85.7% sequence identity with
361 HCO₃⁻ transporters from other terrestrial plant species. Several genes which encode
362 SLC4 family transporters, has been found to be involved in the CCMs in the marine
363 microalgae *Phaeodactylum tricornutum* and *Nannochloropsis oceanica* (Nakajima *et al.*
364 *al.*, 2013; Poliner *et al.*, 2015), as well as the marine macroalga *Ectocarpus siliculosus*
365 (Gravot *et al.*, 2010). More broad evidence from the physiological data have
366 demonstrated that anion exchange proteins play a role in HCO₃⁻ uptake in green, red
367 and brown marine macroalgae (Drechsler *et al.*, 1993; Granbom and Pedersén, 1999;
368 Larsson and Axelsson, 1999; Fernández *et al.*, 2014). Although HCO₃⁻ use by
369 seagrasses is known to involve an anion exchange protein, to our knowledge, this is the
370 first report that provides evidence of the presence of a direct HCO₃⁻ uptake via DIDS-
371 sensitive SLC4 HCO₃⁻ transporters in an aquatic angiosperm. Whatever, these

372 transporters for direct HCO_3^- acquisition, appears to be much more restricted in
373 distribution than the widespread external CA.

374 Three mechanisms of HCO_3^- use have been proposed in aquatic plants: i) indirect
375 use of HCO_3^- based on dehydration of HCO_3^- , facilitated by external CA, to produce
376 elevated CO_2 concentrations outside the plasmalemma; ii) direct uptake of HCO_3^- by
377 an anion exchange transporter in the plasmalemma and iii) direct uptake of HCO_3^- by a
378 P-type H^+ -ATPase (Giordano *et al.*, 2005). In this study we provide evidence for the
379 first two mechanisms in *O. alismoides*. Although we did not specifically check for a P-
380 type H^+ -ATPase, this process appears to be absent, or of minor importance, in *O.*
381 *alismoides* in contrast to *Laminaria digitata* and *L. saccharina* (Klenell *et al.*, 2004),
382 because in *O. alismoides*, HCO_3^- use was abolished by addition of either AZ or DIDS.
383 An AE is mainly responsible for HCO_3^- use in the brown marine macroalga *Macrocystis*
384 *pyrifera* (Fernández *et al.*, 2014), while in several other brown macroalgae such as
385 *Saccharina latissima* (formerly *Laminaria saccharina*) external CA plays the major
386 role in HCO_3^- use (Axelsson *et al.*, 2000), though in *L. saccharina* as in *L. digitata*, a
387 P-type H^+ -ATPase has been identified (Klenell *et al.*, 2004). In another brown
388 macroalga, *Endarachne binghamiae*, HCO_3^- use was based on an external CA and P-
389 type H^+ -ATPase with no contribution from an AE (Zhou and Gao, 2010). Another
390 strategy to use HCO_3^- has been shown in some species of freshwater macrophytes that
391 involves the possession of ‘polar leaves’ (Steemann-Nielsen, 1947). At the lower
392 surface of these leaves, proton extrusion generates low pH and at their upper surface,
393 high pH often generates calcite precipitation (Prins *et al.*, 1980). Consequently, at the
394 lower surface with low pH, the conversion of HCO_3^- to CO_2 near the plasmalemma
395 facilitates the cells to take up C_i . Because of this, there is some evidence for a lower
396 reliance on external CA in macrophytes with polar leaves. For example, in a species
397 with polar leaves, *Potamogeton lucens*, external CA was absent (Staal *et al.*, 1989) and
398 in the polar leaf species *Elodea canadensis*, external CA activity was present but not
399 influenced by the CO_2 concentration (Elzenga and Prins, 1988).

400 It was initially surprising that AZ completely inhibited HCO_3^- use. However,
401 Sterling *et al.* (2001) also found that AZ inhibited AE1-mediated chloride-bicarbonate
402 exchange. This result could be explained by the binding of CA to the AE resulting in
403 the formation of a transport metabolon, where there was a direct transfer of HCO_3^- from
404 CA active site to the HCO_3^- transporter (Sowah and Casey, 2011; Thornell and

405 Bevensee, 2015). Thus, when CA is inhibited, then the transport of HCO_3^- is inhibited.

406 *O. alismoides* can perform C4 photosynthesis, however the final CO_2 concentration
407 at the end of pH-drift, when HCO_3^- -use was abolished by the inhibitors, was 0.8-1.6
408 μM , which could be supported by passive entry of CO_2 without the need to invoke a
409 CCM. These are slightly higher than the CO_2 compensation point in the freshwater C4
410 macrophyte *Hydrilla verticillata* at less than 10 ppm (Bowes, 2010), which is
411 equivalent to a dissolved CO_2 $\sim 0.3 \mu\text{M}$ at 25 °C. If this difference between the species
412 is real and not methodological, it could suggest that in *O. alismoides* C4 photosynthesis
413 is more important to suppress photorespiration than to uptake carbon.

414 A simple model of carbon acquisition (Fig. 7A) was constructed to quantify the
415 contribution of the three pathways involved in C_i uptake in *O. alismoides*: passive
416 diffusion of CO_2 , HCO_3^- -use involving $\alpha\text{CA-1}$ and HCO_3^- -use involving SLC4 HCO_3^-
417 transporters. Using the C_i uptake rates at different CO_2 concentrations in Fig. 3, and
418 assuming that 0.3 mM DIDS completely inhibited HCO_3^- transporters and that 0.2 mM
419 AZ completely inhibited $\alpha\text{CA-1}$ and HCO_3^- transporters, we calculated: i) passive
420 diffusion of CO_2 as the rate in the 0.2 mM AZ treatment that inhibited both $\alpha\text{CA-1}$ and
421 SLC4 HCO_3^- transporters; ii) diffusion of HCO_3^- and conversion to CO_2 by $\alpha\text{CA-1}$ at
422 the plasmalemma as the difference between the rate in the presence of 0.3 mM DIDS
423 and that in the presence of 0.2 mM AZ; and iii) diffusion of HCO_3^- and transfer across
424 the plasmalemma by SLC4 HCO_3^- transporters as the difference in the rate between the
425 control and the 0.3 mM DIDS treatment. At a CO_2 concentration of about 50 μM ,
426 passive diffusion of CO_2 contributed 55.7% to total C_i uptake, diffusion of HCO_3^- and
427 conversion to CO_2 by $\alpha\text{CA-1}$ contributed 42.7% and transfer of HCO_3^- across the
428 plasmalemma by SLC4 HCO_3^- transporters contributed 1.6% (Fig. 7B). At $\sim 9 \mu\text{M}$
429 (about 66% of equilibrium with air at 400 ppm CO_2) the contribution to total C_i uptake
430 of CO_2 -diffusion, HCO_3^- diffusion and conversion to CO_2 by $\alpha\text{CA-1}$ and transfer by
431 SLC4 HCO_3^- transporters was 24.0%, 64.4% and 11.5% respectively and at about 1 μM
432 CO_2 (close to a typical C3 CO_2 compensation point) diffusion was zero and $\alpha\text{CA-1}$ and
433 SLC4 HCO_3^- transporters contributed equally to carbon uptake. So, as CO_2
434 concentrations fall, passive CO_2 diffusion can no longer support C_i uptake and indirect
435 and direct use of HCO_3^- allows C_i uptake to continue. The stimulation of absolute rates
436 of SLC4 HCO_3^- transporters-dependent C_i uptake is consistent with patterns seen for a
437 number of freshwater macrophytes during pH-drift experiments, where rates increase

438 as CO₂ approaches zero before declining as Ci is strongly depleted (Maberly and
439 Spence, 1983). This could be caused by regulation or by direct effects of pH on HCO₃⁻
440 transporters activity.

441 These results confirm the prevailing notion from seagrasses that external CA plays
442 an important role in contributing to Ci uptake. External CA contributed 25% to Ci
443 uptake in *Posidonia australis* (James and Larkum, 1996) and ~60% in *Zostera marina*
444 (approximately 2.2 mM Ci at pH 8.2, equivalent to a dissolved CO₂ ~23 μM at 25 °C;
445 Beer and Rehnberg, 1997), albeit in the presence of Tricine buffer that might inhibit the
446 photosynthesis rate. The value reported here for *O. alismoides* at a CO₂ concentration
447 of 23 μM, 56%, is similar to *Z. marina*.

448 In conclusion, *O. alismoides* has developed a jack of trades CCM, the master of
449 which, either external CA or SLC4 HCO₃⁻ transporters, depends on the CO₂
450 concentration. There are several future lines of work that need to be pursued. The
451 distribution of HCO₃⁻ transporters in freshwater species should be determined. The
452 apparent relationship between polar leaves and low or absent external CA activity could
453 be tested using a range of species, especially within the genus *Ottelia* where calcite
454 precipitation differs among species (Cao *et al.*, 2019). The Ci acquisition mechanisms
455 of more freshwater species should be examined. The cause of the increasing rate of
456 HCO₃⁻ transporters-dependent HCO₃⁻ uptake as Ci becomes depleted needs to be
457 understood. Finally, production and analysis of genome sequences for freshwater
458 macrophytes will be a powerful tool to answer these and future questions concerning
459 the strategies used by freshwater macrophytes to optimize photosynthesis.

460 **Supplementary data**

461 Fig. S1. Commercial CA was used as a positive control and to check activity linearity.

462 Fig. S2. The Ci uptake rate vs the CO₂ concentration at which that rate occurred in *O.*
463 *alismoides* treated without (control) or with inhibitors (AZ and DIDS).

464 Fig. S3. Amino acid sequences of peptides for putative carbonic anhydrase and
465 bicarbonate transporters from *O. alismoides*.

466 Table S1. Information on the different CO₂ acclimation experiments.

467 **Acknowledgements**

468 This work was supported by the Strategic Priority Research Program of the Chinese
469 Academy of Sciences (Grant No. XDB31000000), Chinese Academy of Sciences
470 President's International Fellowship Initiative to SCM and BG (2015VBA023,
471 2016VBA006), and the National Natural Science Foundation of China (Grant No.
472 31970368).

473

References

- Axelsson L, Mercado JM, Figueroa FL.** 2000. Utilization of HCO_3^- at high pH by the brown macroalga *Laminaria saccharina*. *European Journal of Phycology* **35**, 53–59.
- Bauer H, Martha P.** 1981. The CO_2 compensation point of C_3 plants-A re-examination I. Interspecific variability. *Zeitschrift für Pflanzenphysiologie* **103**, 445–450.
- Beer S, Rehnberg J.** 1997. The acquisition of inorganic carbon by the seagrass *Zostera marina*. *Aquatic Botany* **56**, 277–283.
- Björk M, Weil A, Semesi S, Beer S.** 1997. Photosynthetic utilization of inorganic carbon by seagrasses from Zanzibar, East Africa. *Marine Biology* **129**, 363–366.
- Black MA, Maberly SC, Spence DHN.** 1981. Resistance to carbon dioxide fixation in four submerged freshwater macrophytes. *New Phytologist* **89**, 557–568.
- Bowes G.** 2010. Chapter 5 Single-Cell C_4 Photosynthesis in Aquatic Plants. In: Raghavendra A, Sage R. (eds) *C_4 Photosynthesis and Related CO_2 Concentrating Mechanisms*. *Advances in Photosynthesis and Respiration* **32**, 63–80. Springer, Dordrecht.
- Cabantchik ZI, Greger R.** 1992. Chemical probes for anion transporters of mammalian cell membranes. *American Journal of Physiology* **262**, C803–C827.
- Cao Y, Liu Y, Ndirangu L, Li W, Xian L, Jiang HS.** 2019. The analysis of leaf traits of eight *Ottelia* populations and their potential ecosystem functions in Karst freshwaters in China. *Frontiers in Plant Science* **9**, 1938.
- Clement R, Lignon S, Mansuelle P, Jensen E, Pophillat M, Lebrun R, Denis Y, Puppo C, Maberly SC, Gontero B.** 2017. Responses of the marine diatom *Thalassiosira pseudonana* to changes in CO_2 concentration: a proteomic approach. *Scientific Reports* **7**, 42333.
- Denny P, Weeks DC.** 1970. Effects of light and bicarbonate on membrane potential in *Potamogeton schweinfurthii* (Benn). *Annals of Botany* **34**, 483–496.
- DiMario RJ, Machingura MC, Waldrop GL, Moroney JV.** 2018. The many types of carbonic anhydrases in photosynthetic organisms. *Plant Science* **268**, 11–17.
- Drechsler Z, Sharkia R, Cabantchik ZI, Beer S.** 1993. Bicarbonate uptake in the marine macroalga *Ulva* sp. is inhibited by classical probes of anion exchange by red blood cells. *Planta* **191**, 34–40.

- Elzenga JTM, Prins HBA.** 1988. Adaptation of *Elodea* and *Potamogeton* to different inorganic carbon levels and the mechanism for photosynthetic bicarbonate utilization. *Australian Journal of Plant Physiology* **15**, 727–735.
- Emanuelsson O, Brunak S, von Heijne G, Nielsen H.** 2007. Locating proteins in the cell using TargetP, SignalP and related tools. *Nature Protocol* **2**, 953–971.
- Fernández PA, Hurd CL, Roleda MY.** 2014. Bicarbonate uptake via an anion exchange protein is the main mechanism of inorganic carbon acquisition by the giant kelp *Macrocystis pyrifera* (Laminariales, Phaeophyceae) under variable pH. *Journal of Phycology* **50**, 998–1008.
- Fernández PA, Roleda MY, Rautenberger R, Hurd CL.** 2018. Carbonic anhydrase activity in seaweeds: overview and recommendations for measuring activity with an electrometric method, using *Macrocystis pyrifera* as a model species. *Marine Biology* **165**, 88.
- Fujiwara S, Fukuzawa H, Tachiki A, Miyachi S.** 1990. Structure and differential expression of 2 genes encoding carbonic-anhydrase in *Chlamydomonas reinhardtii*. *Proceedings of the National Academy of Sciences USA* **87**, 9779–9783.
- Giordano M, Beardall J, Raven JA.** 2005. CO₂ concentrating mechanisms in algae: mechanisms, environmental modulation, and evolution. *Annual Review of Plant Biology* **56**, 99–131.
- Granbom M, Pedersén M.** 1999. Carbon acquisition strategies of the red alga *Euclima denticulatum*. *Hydrobiologia* **398/399**, 349–354.
- Gravot A, Dittami SM, Rousvoal S, Lugan R, Eggert A, Collen J, Boyen C, Bouchereau A, Tonon T.** 2010. Diurnal oscillations of metabolite abundances and gene analysis provide new insights into central metabolic processes of the brown alga *Ectocarpus siliculosus*. *New Phytologist* **188**, 98–110.
- Hackl T, Hedrich R, Schultz J, Förster F.** 2014. Proovread: large-scale high-accuracy pacbio correction through iterative short read consensus. *Bioinformatics* **30**, 3004–3011.
- Han SJ, Maberly SC, Gontero B, Xing ZF, Li W, Jiang HS, Huang WM.** 2020. Structural basis for C₄ photosynthesis without Kranz anatomy in leaves of the submerged freshwater plant *Ottelia alismoides*. *Annals of Botany* doi: <https://doi.org/10.1093/aob/mcaa005>
- Harada H, Matsuda Y.** 2005. Identification and characterization of a new carbonic

- anhydrase in the marine diatom *Phaeodactylum tricorutum*. Canadian Journal of Botany **83**, 909–916.
- Harada H, Nakatsuma D, Ishida M, Matsuda Y.** 2005. Regulation of the expression of intracellular β -carbonic anhydrase in response to CO₂ and light in the marine diatom *Phaeodactylum tricorutum*. Plant Physiology **139**, 1041–1050.
- Huang WM, Shao H, Zhou SN, Zhou Q, Fu WL, Zhang T, Jiang HS, Li W, Gontero B, Maberly SC.** 2018. Different CO₂ acclimation strategies in juvenile and mature leaves of *Ottelia alismoides*. Photosynthesis Research **138**, 219–232.
- Iversen LL, Winkel A, Baastrup-Spohr L, Hinke AB, Alahuhta J, Baatrup-Pedersen A, Birk S, Brodersen P, Chambers PA, Ecke F, Feldmann T, Gebler D, Heino J, Jespersen TS, Moe SJ, Riis T, Sass L, Vestergaard O, Maberly SC, Sand-Jensen K, Pedersen O.** 2019. Catchment properties and the photosynthetic trait composition of freshwater plant communities. Science **366**, 878–881.
- James PL, Larkum AWD.** 1996. Photosynthetic inorganic carbon acquisition of *Posidonia australis*. Aquatic Botany **55**, 149–157.
- Jensen EL, Clement R, Kosta A, Maberly SC, Gontero B.** 2019. A new widespread subclass of carbonic anhydrase in marine phytoplankton. The ISME Journal **13**, 2094–2106.
- Karlsson J, Clarke AK, Chen ZY, Huggins SY, Park YI, Husic HD, Moroney JV, Samuelsson G.** 1998. A novel alpha-type carbonic anhydrase associated with the thylakoid membrane in *Chlamydomonas reinhardtii* is required for growth at ambient CO₂. EMBO Journal **17**, 1208–1216.
- Klavnsen SK, Madsen TV, Maberly SC.** 2011. Crassulacean acid metabolism in the context of other carbon-concentrating mechanisms in freshwater plants: a review. Photosynthesis Research **109**, 269–279.
- Klenell M, Snoeijs P, Pedersén M.** 2004. Active carbon uptake in *Laminaria digitata* and *L. saccharina* (Phaeophyta) is driven by a proton pump in the plasma membrane. Hydrobiologia **514**, 41–53.
- Larsson C, Axelsson L.** 1999. Bicarbonate uptake and utilization in marine macroalgae. European Journal of Phycology **34**, 79–86.
- Maberly SC, Spence DHN.** 1983. Photosynthetic inorganic carbon use by freshwater plants. Journal of Ecology **71**, 705–724.
- Maberly SC.** 1990. Exogenous sources of inorganic carbon for photosynthesis by

- marine macroalgae. *Journal of Phycology* **26**, 439–449.
- Maberly SC.** 1996. Diel, episodic and seasonal changes in pH and concentrations of inorganic carbon in a productive lake. *Freshwater Biology* **35**, 579–598.
- Maberly SC, Madsen TV.** 1998. Affinity for CO₂ in relation to the ability of freshwater macrophytes to use HCO₃⁻. *Functional Ecology* **12**, 99–106.
- Maberly SC, Gontero B.** 2017. Ecological imperatives for aquatic CO₂-concentrating mechanisms. *Journal of Experimental Botany* **68**, 3797–3814.
- Maberly SC, Gontero B.** 2018. Trade-offs and synergies in the structural and functional characteristics of leaves photosynthesizing in aquatic environments. In: Adams III WW, Terashima I. (eds.) *The leaf: a platform for performing photosynthesis. Advances in photosynthesis and respiration (Including bioenergy and related processes)*. Springer, Cham. 307–343.
- Millhouse J, Strother S.** 1986. Salt-stimulated bicarbonate-dependent photosynthesis in the marine angiosperm *Zostera muelleri*. *Journal of Experimental Botany* **37**, 965–976.
- Moroney JV, Husic HD, Tolbert NE.** 1985. Effect of carbonic anhydrase inhibitors on inorganic carbon accumulation by *Chlamydomonas reinhardtii*. *Plant Physiology* **79**, 177–183.
- Moroney JV, Chen ZY.** 1998. The role of the chloroplast in inorganic carbon uptake by eukaryotic algae. *Canadian Journal of Botany* **76**, 1025–1034.
- Moroney JV, Bartlett SG, Samuelsson G.** 2001. Carbonic anhydrases in plants and algae. *Plant Cell & Environment* **24**, 141–153.
- Moroney JV, Ma Y, Frey WD, Fusilier KA, Pham TT, Simms TA, DiMario RJ, Yang J, Mukherjee B.** 2011. The carbonic anhydrase isoforms of *Chlamydomonas reinhardtii*: intracellular location, expression, and physiological roles. *Photosynthesis Research* **109**, 133–149.
- Nakajima K, Tanaka A, Matsuda Y.** 2013. SLC4 family transporters in a marine diatom directly pump bicarbonate from seawater. *Proceedings of the National Academy of Sciences USA* **110**, 1767–1772.
- Poliner E, Panchy N, Newton L, Wu G, Lapinsky A, Bullard B, Zienkiewicz A, Benning C, Shiu SH, Farré EM.** 2015. Transcriptional coordination of physiological responses in *Nannochloropsis oceanica* CCM1779 under light/dark cycles. *Plant Journal* **83**, 1097–1113.

- Prins HBA, Snel JFH, Helder RJ, Zanstra PE.** 1980. Photosynthetic HCO_3^- utilization and OH^- excretion in aquatic angiosperms: light induced pH changes at the leaf surface. *Plant Physiology* **66**, 818–822.
- Raven JA.** 1970. Exogenous inorganic carbon sources in plant photosynthesis. *Biological Reviews* **45**, 167–221.
- Roberts RJ, Carneiro MO, Schatz MC.** 2013. The advantages of SMRT sequencing. *Genome Biology* **14**, 405.
- Romero MF, Chen AP, Parker MD, Boron WF.** 2013. The SLC4 family of bicarbonate (HCO_3^-) transporters. *Molecular Aspects of Medicine* **34**, 159–182.
- Samukawa M, Shen C, Hopkinson BM, Matsuda Y.** 2014. Localization of putative carbonic anhydrases in the marine diatom, *Thalassiosira pseudonana*. *Photosynthesis Research* **121**, 235–249.
- Satoh D, Hiraoka Y, Colman B, Matsuda Y.** 2001. Physiological and molecular biological characterization of intracellular carbonic anhydrase from the marine diatom *Phaeodactylum tricorutum*. *Plant Physiology* **126**, 1459–1470.
- Shao H, Gontero B, Maberly SC, Jiang HS, Cao Y, Li W, Huang WM.** 2017. Responses of *Ottelia alismoides*, an aquatic plant with three CCMs, to variable CO_2 and light. *Journal of Experimental Botany* **68**, 3985–3995.
- Sharkia R, Beer S, Cabantchik ZI.** 1994. A membrane-located polypeptide of *Ulva* sp. which may be involved in HCO_3^- uptake is recognized by antibodies raised against the human red-blood-cell anion-exchange protein. *Planta* **194**, 247–249.
- Silva TSF, Melack JM, Novo EMLM.** 2013. Responses of aquatic macrophyte cover and productivity to flooding variability on the Amazon floodplain. *Global Change Biology* **19**, 3379–3389.
- Sowah D, Casey JR.** 2011. An intramolecular transport metabolon: fusion of carbonic anhydrase II to the COOH terminus of the $\text{Cl}^-/\text{HCO}_3^-$ exchanger, AE1. *American Journal of Physiology-Cell Physiology* **301**, C336–C346.
- Staal M, Elzenga JTM, Prins HBA.** 1989. ^{14}C fixation by leaves and leaf cell protoplasts of the submerged aquatic angiosperm *Potamogeton lucens*: carbon dioxide or bicarbonate? *Plant Physiology* **90**, 1035–1040.
- Steemann-Nielsen E.** 1947. Photosynthesis of aquatic plants with special reference to the carbon sources. *Dansk Botanisk Arkiv Udgivet af Dansk Botanisk Forening* **8**, 3–71.

- Sterling D, Reithmeier RAF, Casey JR.** 2001. A transport metabolon: Functional interaction of carbonic anhydrase II and chloride/bicarbonate exchangers. *The Journal of Biological Chemistry* **276**, 47886–47894.
- Tachibana M, Allen AE, Kikutani S, Endo Y, Bowler C, Matsuda Y.** 2011. Localization of putative carbonic anhydrases in two marine diatoms, *Phaeodactylum tricornutum* and *Thalassiosira pseudonana*. *Photosynthesis Research* **109**, 205–221.
- Thornell IM, Bevenssee MO.** 2015. Regulators of *Slc4* bicarbonate transporter activity. *Frontiers in Physiology* **6**, 166.
- Tsuji Y, Nakajima K, Matsuda Y.** 2017. Molecular aspects of the biophysical CO₂-concentrating mechanism and its regulation in marine diatoms. *Journal of Experimental Botany* **68**, 3763–3772.
- van Hille R, Fagan M, Bromfield L, Pott R.** 2014. A modified pH drift assay for inorganic carbon accumulation and external carbonic anhydrase activity in microalgae. *Journal of Applied Phycology* **26**, 377–385.
- Zhang YZ, Yin LY, Jiang HS, Li W, Gontero B, Maberly SC.** 2014. Biochemical and biophysical CO₂ concentrating mechanisms in two species of freshwater macrophyte within the genus *Ottelia* (Hydrocharitaceae). *Photosynthesis Research* **121**, 285–297.
- Zou DH, Gao KS.** 2010. Acquisition of inorganic carbon by *Endarachne binghamiae* (Scytosiphonales, Phaeophyceae). *European Journal of Phycology* **45**, 117–126.

Figure legends

Figure 1. Example of a typical pH-drift over time (one replicate) for *O. alismoides* tested at an initial alkalinity of 1 mequiv L⁻¹ without (control) or with inhibitors (AZ, DIDS).

Figure 2. Analysis of pH drift experiments without (control) or with inhibitors (AZ and DIDS) in *O. alismoides*. (A) Final pH; (B) Final CO₂ concentration; (C) Initial slope of Ci uptake rate vs concentration of CO₂ (between 15~40 μM), α_C; (D) CO₂ compensation point (CP(CO₂)); (E) C_T/Alk. Values represent means ± SE, n=3. Letters indicate statistical differences between control and treatments (one-way ANOVA, Duncan's and Tukey's post-hoc tests P<0.05).

Figure 3. Effect of AZ or DIDS on the Ci uptake rate at different CO₂ concentrations in *O. alismoides*. (A) Ci uptake rate; (B) Ci uptake inhibition. Values represent means ± SE, n=3. Letters in (A) indicate statistical differences among control and inhibitor treatments within CO₂ concentrations (one-way ANOVA, Duncan's and Tukey's post-hoc tests P<0.05). Letters and symbols in (B) indicate statistical differences among different CO₂ concentrations within inhibitor treatment (Mann-Whitney test P<0.05).

Figure 4. Effect of removal of AZ on Ci uptake rate in *O. alismoides* leaves at different CO₂ concentrations. Values represent means ± SE, n=3. (A) 0.1 mM AZ; (B) 0.2 mM AZ. The inhibitor was removed by washing the treated leaves in the post-control (see Methods). Letters indicate statistical differences between the control and inhibitor treatments of AZ for each CO₂ concentration (one-way ANOVA, Duncan's and Tukey's post-hoc tests P<0.05).

Figure 5. Effect of AZ and DIDS on Ci uptake rate and external CA activity in leaves of *O. alismoides* acclimated to high CO₂ (HC) or low CO₂ (LC) and measured at an initial CO₂ concentration of 12 μM. (A) Ci uptake rate; (B) Inhibition of Ci uptake rate;

(C) External CA activity and (D) Inhibition of external CA activity. Values represent means \pm SE, n=3. For panels (A) and (C), letters indicate statistical differences between the control and different treatments at HC and LC acclimated leaves using one-way ANOVA, Duncan's and Tukey's post-hoc tests $P < 0.05$. For panels (B) and (D), uppercase and lowercase letters indicate statistical differences among inhibitor treatments at HC and LC respectively using the Mann–Whitney test $P < 0.05$; the line above the two columns indicates the statistical differences between HC and LC treatments (Mann–Whitney test $P < 0.05$).

Figure 6. Phylogenetic tree of α CA-1 isoforms, prediction of location for α CA-1 peptides, and mRNA expression for α CA-1 and SLC4 HCO_3^- transporters in *O. alismoides* leaves acclimated at high CO_2 (HC) and low CO_2 (LC) concentrations. (A) Phylogenetic tree of α CA-1 isoforms in *O. alismoides*; (B) Output of the predicted location tested on the four isoforms for putative α CA-1 from the Target P server; (C) mRNA expression for α CA-1; (D) mRNA expression for SLC4 HCO_3^- transporters. In panel (A), the scale bar at the bottom represents the evolutionary distances in amino acid sequences. In panel (B), cTP is the chloroplast transit peptide, mTP is the mitochondrial targeting peptide, SP is the secretory pathway, Other stands for other locations, Loc gives the final prediction, RC is the reliability class (from 1 to 5), where 1 indicates the strongest prediction. The default was used to choose cutoffs for the predictions. Values in panels (C) and (D) represent the mean \pm SE, n=3. Data of SLC4 HCO_3^- transporters expression in panel (D) correspond to the highest expressed transcript. The lines in panels (C) and (D) above the two columns indicate the statistical differences between LC and HC treatment (one-way ANOVA, $P < 0.05$).

Figure 7. A model of inorganic carbon acquisition in *O. alismoides*. (A) Model structure. ① passive diffusion of CO_2 ; ② diffusion of HCO_3^- and conversion to CO_2 by α CA-1 at the plasmalemma; ③ diffusion of HCO_3^- and transfer across the plasmalemma by SLC4 HCO_3^- transporters. (B) The contribution of CO_2 -diffusion, diffusion of HCO_3^-

and conversion to CO_2 via $\alpha\text{CA-1}$ and transfer of HCO_3^- by SLC4 HCO_3^- transporters to total C_i uptake at different CO_2 concentrations.

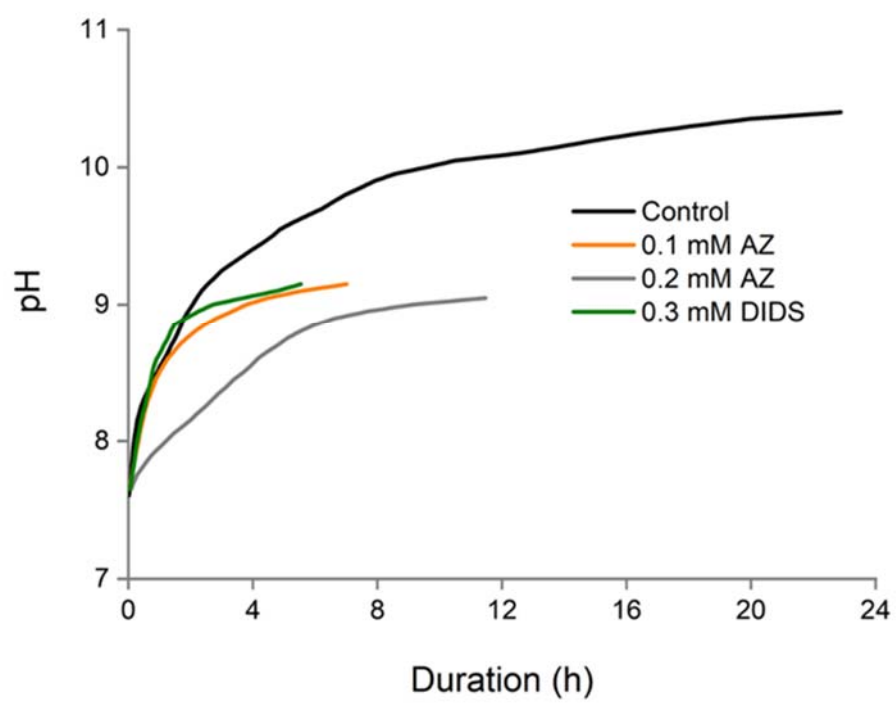


Figure 1

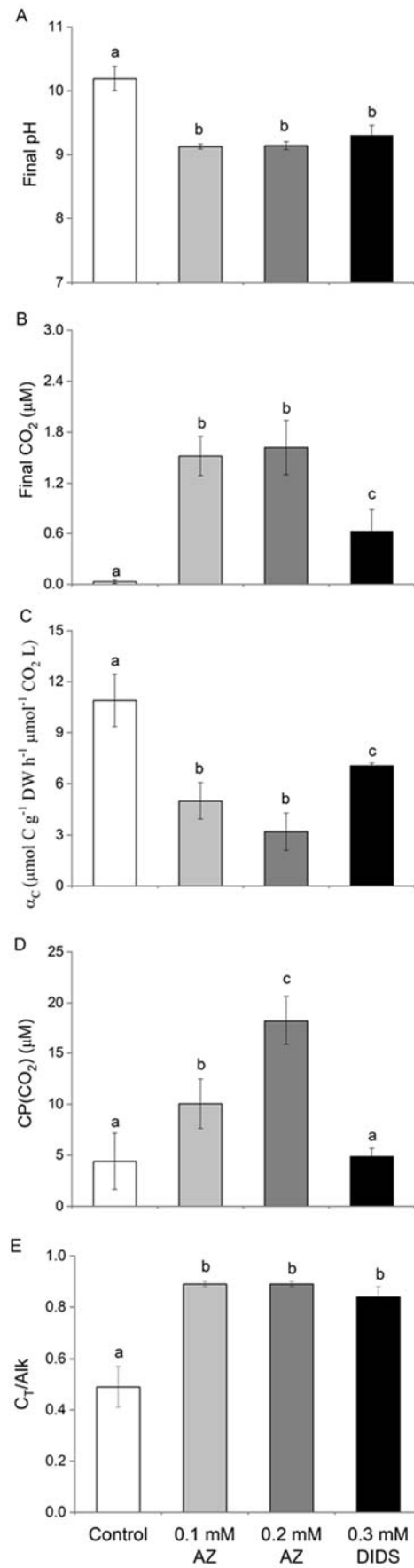


Figure 2

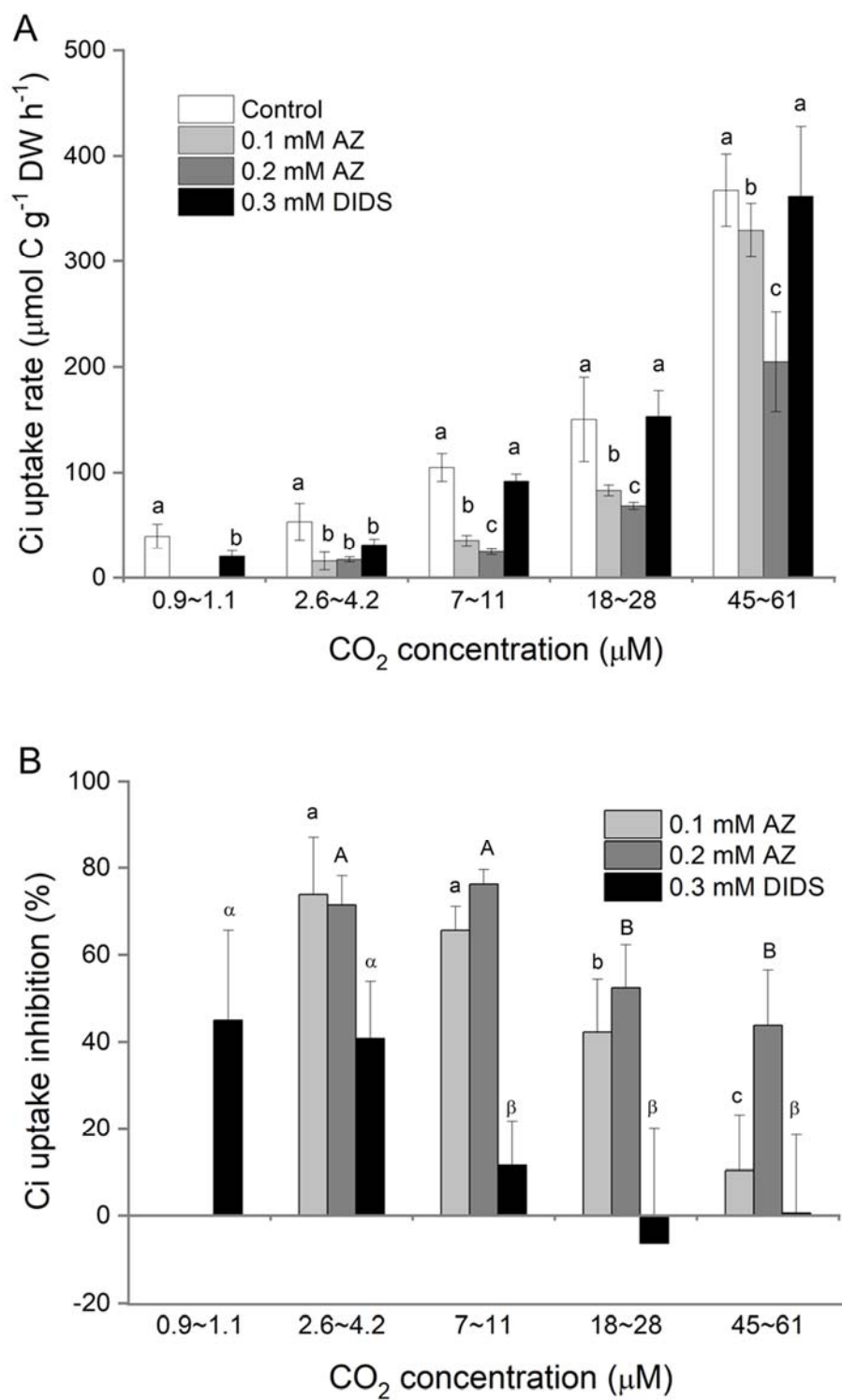


Figure 3

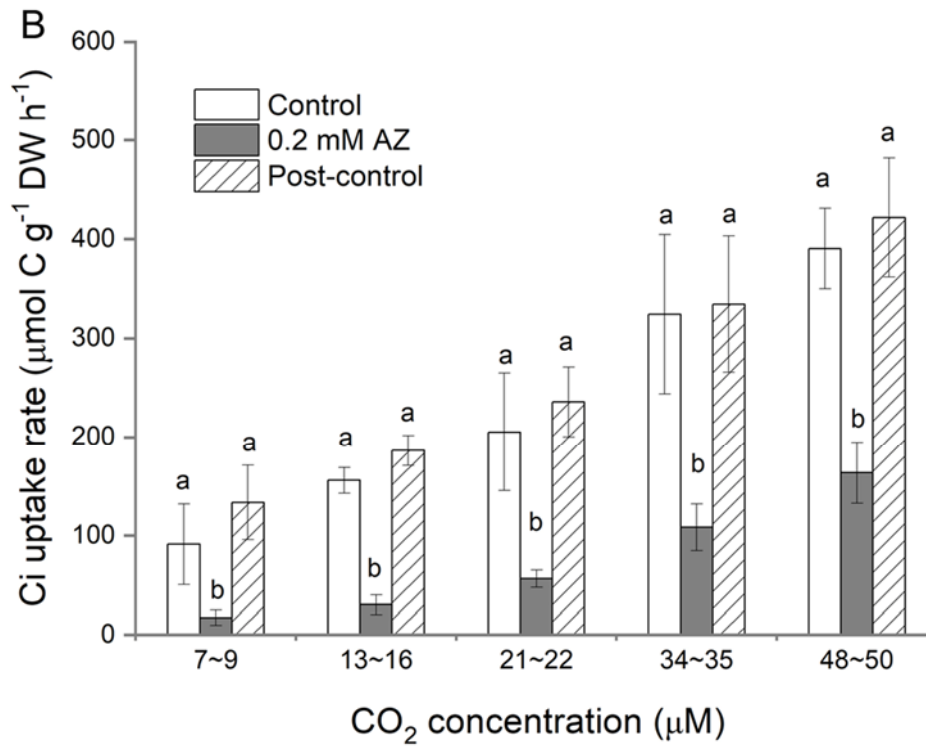
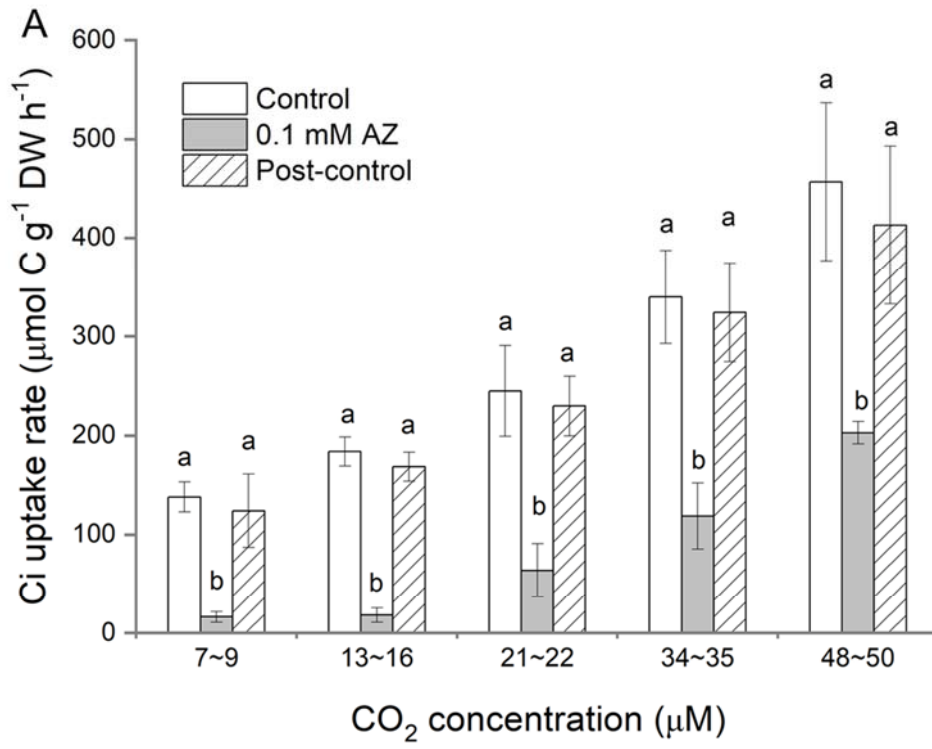


Figure 4

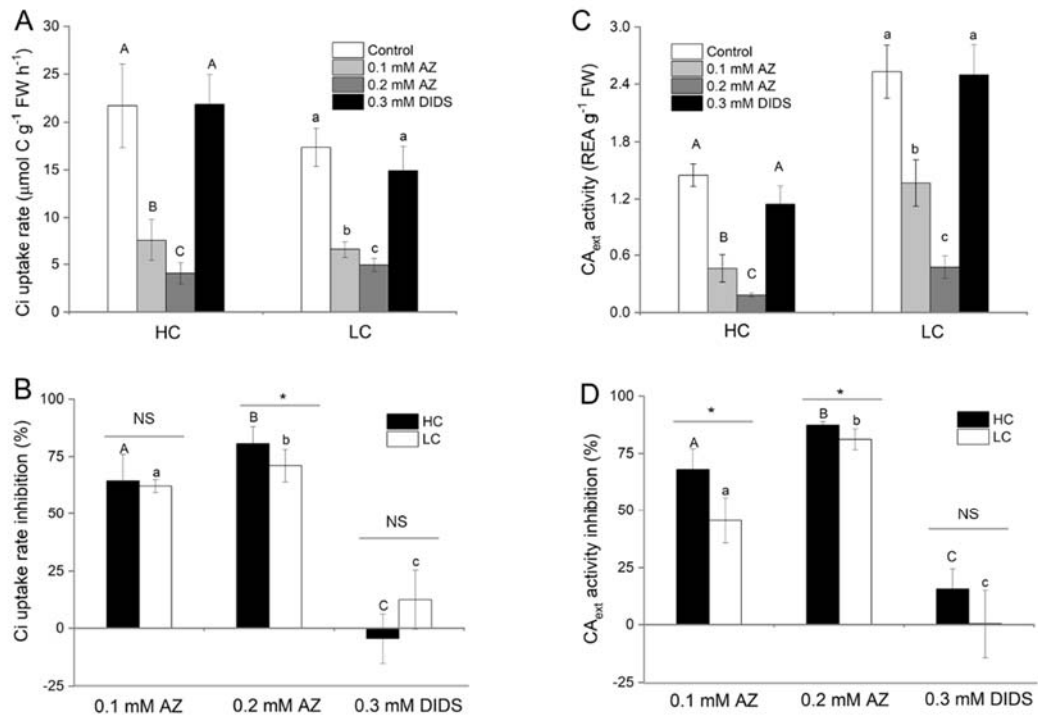
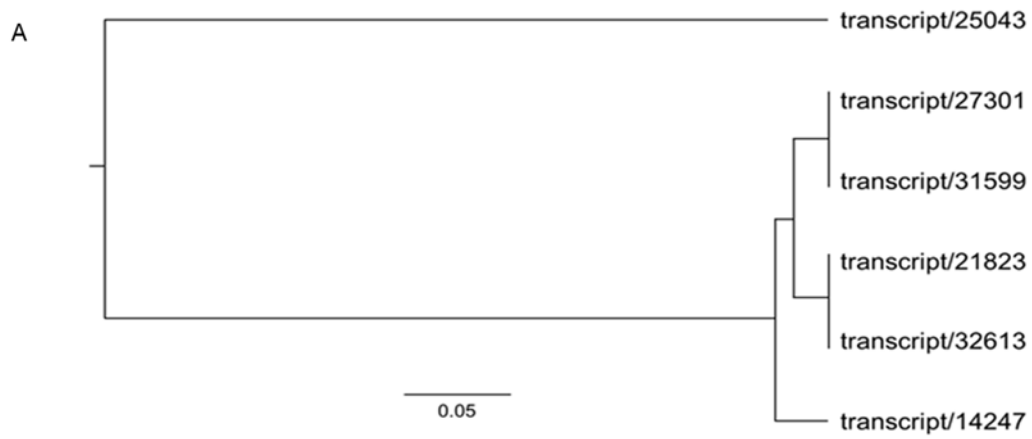


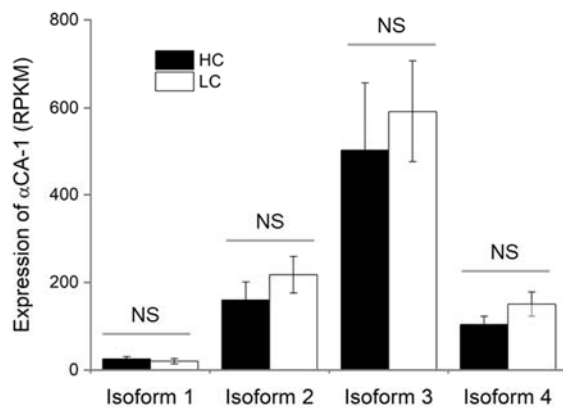
Figure 5



B

Putative protein	Isoforms	cTP	mTP	SP	Other	Loc	RC
α CA-1	1	0.077	0.025	0.885	0.013	SP	1
α CA-1	2	0.023	0.023	0.951	0.050	SP	1
α CA-1	3	0.021	0.025	0.952	0.054	SP	1
α CA-1	4	0.023	0.023	0.951	0.050	SP	1

C



D

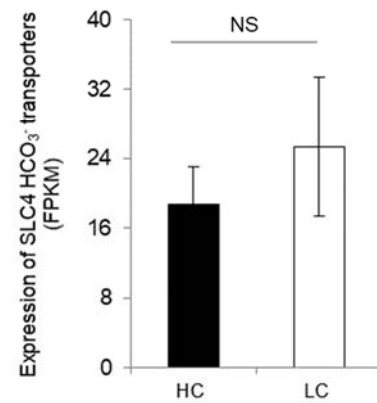


Figure 6

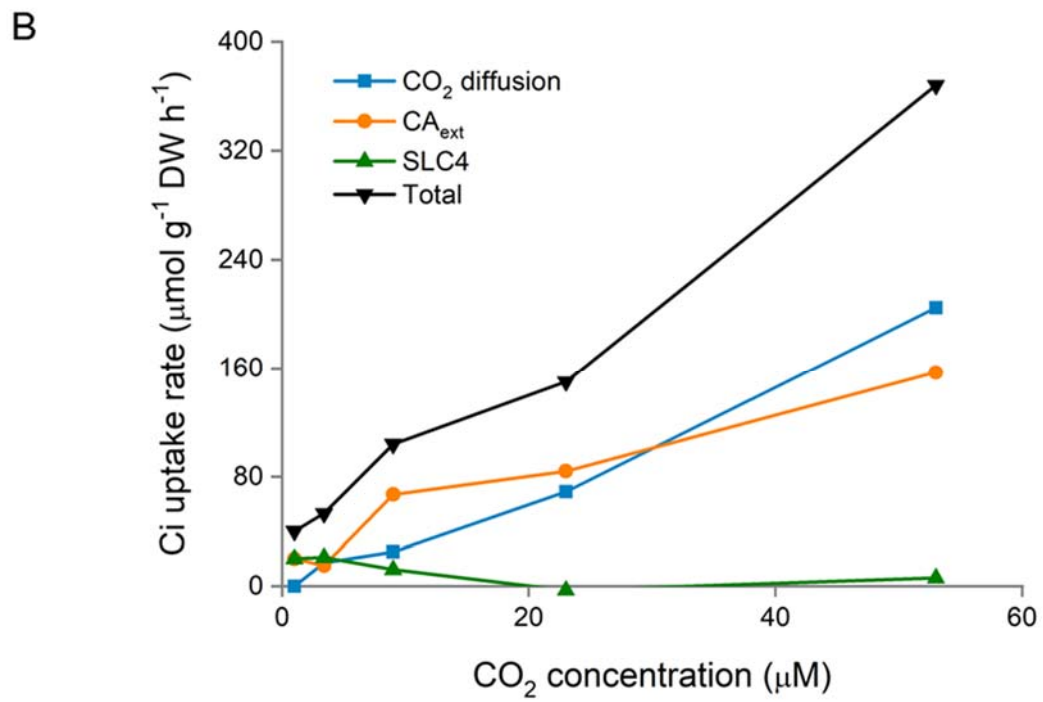
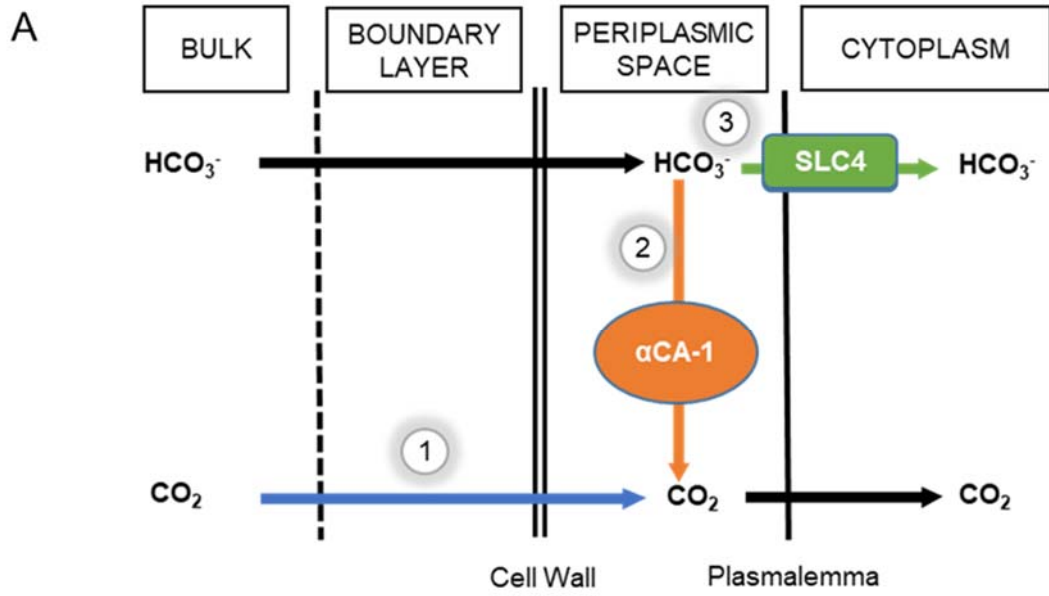


Figure 7